

## 3D COMPUTER MODEL OF THE Co-Cu-CoS-Cu<sub>2</sub>S SUBSYSTEM T-X-Y DIAGRAM ABOVE 800°C

V. I. Lutsyk <sup>a,b,\*</sup>, V. P. Vorob'eva <sup>a</sup>, A. E. Zelenaya <sup>a</sup>, M. V. Lamueva <sup>a</sup>

<sup>a</sup> Institute of Physical Materials Science, Siberian Branch, Russian Academy of Sciences, Ulan-Ude, Russia

<sup>b</sup> Banzarov Buryat State University, Chemical Department, Ulan-Ude, Russia

(Received 07 March 2019; Accepted 30 March 2021)

### Abstract

The three-dimensional computer model of the Co-Cu-CoS-Cu<sub>2</sub>S subsystem T-x-y diagram at temperatures above 800°C is represented. It is shown that the liquid immiscibility in the binary subsystem Cu-Cu<sub>2</sub>S is transformed within the ternary system with Co into the wide two-phase region of two immiscible melts, which interrupts the univariant curve of the Co and Cu<sub>2</sub>S co-crystallization. The special features of the structure of the solidus surface of cobalt, caused by liquid-phase immiscibility are considered.

**Keywords:** Phase diagrams; Immiscibility; 3D visualization; Metal-sulfide systems; Alloys of cobalt and copper

### 1. Introduction

This work was carried out within the framework of the study of three- and four-component systems, which form the five-component Fe-Ni-Co-Cu-S system.

Investigation of this quinary system was declared in the title of the paper [1], but really the study was limited by the only quaternary system Fe-Ni-Cu-S and ternary systems on its borders. As for the systems with cobalt, the only Co-S binary system was discussed. Generally, many publications are devoted to the Fe-Ni-Cu-S system, for instance [1-3]. It is possible especially to name among them the papers [2] and [3], because besides the detailed description of the experiments, the results are represented in the form of three-dimensional (3D) isothermal sections (which occurs infrequently): six isothermal sections in the diapason 700-1200°C in the limited region of concentrations (up to 10 % weight Fe) [2] and 3D isothermal sections at 1000°C, 850°C and 400°C [3].

Furthermore, the theoretical analysis of the Fe-Ni-Cu-S system for the processes of the quasi-equilibrium directional solidification of the four-component melt was carried out [4, 5] and the relationship between the phase diagram and the formation of primary zones in a directionally solidified material was examined [6].

All ternary systems, forming the Fe-Ni-Cu-S system were thoroughly studied in [7] and the results of these experimental studies were represented in the

form of the concentration projections of the surfaces of liquidus and solidus (and the ruled surfaces, produced by their intersection) with isothermal lines.

Among other four-component systems which form the above mentioned five-component one, it is possible to name the papers devoted to the Fe-Ni-Co-Cu [8] and Fe-Ni-Co-S [8, 9] systems.

Information about the results of the experimental study and thermodynamic calculations of the Ni-Cu-S system phase diagram can be found in [10-13] and of the Fe-Cu-S system – in [14-16]. Only isothermal sections at 400-900°C in the Co-Cu-S system are represented in [17], but the problems of the liquid immiscibility were not discussed here.

The authors of [7] studied in detail the ternary systems on the boundaries of the Fe-Ni-Cu-S system, now are carrying out the analogous studies of the Fe-Co-Cu-S system [18-20].

However, the main problem and the main difficulties both in the experimental results representation and in the phase diagrams of ternary and quaternary systems computer simulation are caused by the liquid immiscibility in the binary Cu-S system. Immiscibility in the ternary system formed by the Cu-Cu<sub>2</sub>S binary with Ni produces the univariant monotectic transformation, and with Fe or Co – the invariant one. Unfortunately, there are practically no theoretical works devoted to the influence of the liquid immiscibility on the geometric structure of T-x-y and T-x-y-z diagrams of three- and four-component

Corresponding author: vluts@ipms.bsnet.ru

<https://doi.org/10.2298/JMMB190307028L>



systems [21].

The most complete review of T-x-y diagrams with melt immiscibility can be found in the monograph [22]. It has examples of nine eutectic type diagrams with immiscibility. Five of them are formed by one, two, or three binary systems with monotectic, where a dome of immiscibility: 1) occupies a part of one liquidus field; 2) starts from the binary liquidus and crosses the univariant curve between the two liquidus fields; 3) crosses two fields of liquidus; 4) exists in all three liquidus fields, forming a complex structure of the phase region with three liquids. Four more examples are given for a eutectic system, in which the dome above two liquid phases does not connect the binary systems, but exists in one, two, three fields of liquidus, crossing, respectively, one, two or three univariant curves. In monographs [23, 24], the system made up of binary ones was discussed: with the continuous rows of solid solutions, eutectic and monotectic. As for the diagrams described in [22], the most discussed in other monographs [23, 25-27] is a diagram with invariant monotectic equilibrium.

However, the works [22-27] are not free from flaws. Some of them are mentioned in [28]. It is also important to emphasize that the surface of solidus which is conjugated to the surface of liquidus, into which the immiscibility dome is entering, has geometric features, which are referred to, for example, in [29, 30].

Therefore it is convenient to use the spacious (3D – for ternary and 4D – for quaternary systems) computer models of phase (T-x-y, T-x-y-z) diagrams for visualization and better understanding of the obtained experimental data and general geometric construction of some phase diagrams for specific systems.

The basic approach to construct the spatial models of isobaric phase diagrams of three-component systems is that each of these models is a geometric object of three-dimensional (3D) space in the coordinates of the temperature-concentration (T-x-y), composed of non-ruled and ruled surfaces. Ruled surface is generated by a forming horizontal segment and two directing curves and bounds the corresponding three-phase region. All other surfaces (liquidus, solidus, solvus, transus, etc.) are the non-ruled ones.

It is obvious that the principle of the ruled surface formation corresponds to the kinematic way of its origin. However, this method allows generating adequately the non-ruled surface as the forming element moving along the directing ones, too. Only in this case there are no requirements to the forming element to be straightforward. In cases, when the kinematic method cannot “cover” the entire surface (for example, if there are folds or holes), it is broken into fragments. Then the problem of the surface adequate presentation is connected with its gluing from fragments, with obligatory control by equating derivatives in the places of gluing.

The technology of PD spatial models creating from its geometric elements (surfaces or phase regions) is implemented in the author’s program Phase Diagrams Designer [31].

Papers cited above include isothermal sections (three-dimensional sections for the four-component Fe-Ni-Cu-S system [2, 3]) and sometimes the projection of liquidus [13] and even liquidus and solidus surfaces [7, 18-20]. This limited information does not give the possibility to obtain the phase diagram as a whole, since entire enormous volume of the carried out experimental work is not brought to the total space model, which would make it possible to construct any arbitrarily given sections and perform the calculations of the mass balances of the multiphase compositions which are formed during the crystallization of the quaternary melts.

## 2. Initial experimental data

Binary systems are well studied and reference books data of their phase diagrams can be confidently used [32-34] (Figure 1).

The investigation of the Co-Cu-S system (the Co-Cu-CoS-Cu<sub>2</sub>S subsystem) is limited in the current

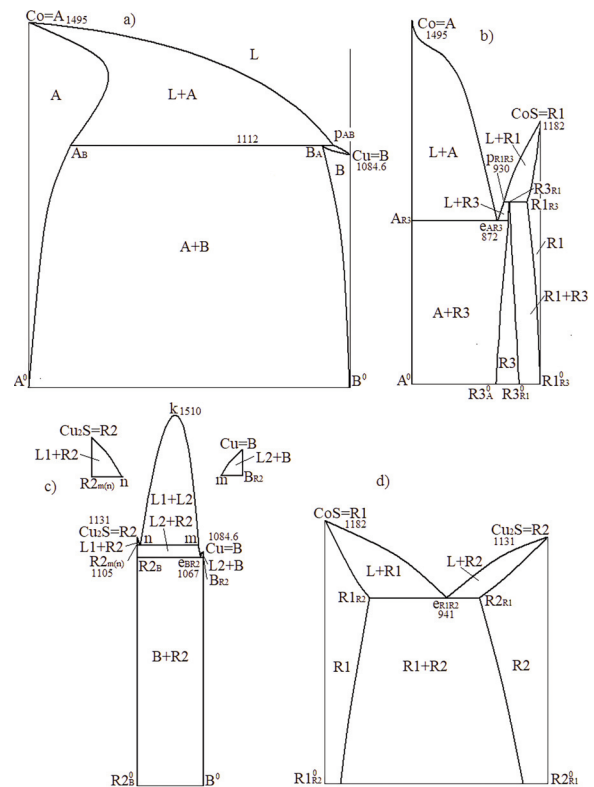


**Figure 1.** Binary systems Co-Cu (A-B) (a), Co-CoS (A-R1) (b), Cu-Cu<sub>2</sub>S (B-R2) with an enlarged fragment of the phase regions L1+R2 and L2+B (c), the quasi-binary section CoS-Cu<sub>2</sub>S (R1-R2) (d), forming the subsystem Co-Cu-CoS-Cu<sub>2</sub>S (A-B-R1-R2)



research in concentration - by the quasi-binary section CoS-Cu<sub>2</sub>S and in temperature - by 800°C (Figure 2).

The design of 3D computer model requires re-designation of initial components and compounds [31]: Co, Cu, CoS, Cu<sub>2</sub>S, Co<sub>4</sub>S<sub>3</sub> as A, B, R1, R2, R3, correspondingly, and then of the basic points which form the phase diagram (Table 1-2). For instance, designations e<sub>BR2</sub>, B<sub>R2</sub>, and R<sub>2B</sub> correspond to the apexes of the invariant complex in the binary Cu-S system (the Cu-Cu<sub>2</sub>S or B-R2 subsystem), i.e., to phases L, Cu (B), and Cu<sub>2</sub>S (R2), participating in the eutectic L→Cu+Cu<sub>2</sub>S (e<sub>BR2</sub>: L→B+R2) reaction.

The binary Co-Cu (A-B) system is the usual peritectic system with one transformation L+Co→Cu (p<sub>AB</sub>: L+A→B) at 1112°C (Figure 1a). It is characterized by the variable solubility of Cu in a-Co. It is observed as a “retrograde” view of the solidus in the temperature range 1112-1495°C, when the solubility of copper in the solid solution first grows with an increase of the temperature, and then it decreases and has a maximum at 1367°C and the concentration of copper 20.8 % weight.

The compound Co<sub>1+x</sub>S (R1) is melted congruently at the temperature of 1182±1°C and is characterized by the region of the homogeneity in the range of concentrations 35.5-40 % weight of sulfur.

The incongruently melting compound Co<sub>4</sub>S<sub>3</sub> (R3) forms in the binary Co-CoS (A-R1) subsystem as a result of the peritectic L+CoS→Co<sub>4</sub>S<sub>3</sub> (p<sub>R1R3</sub>: L+R1→R3) reaction at 930°C. The eutectic L→Co+Co<sub>4</sub>S<sub>3</sub> (e<sub>AR3</sub>: L→A+R3) reaction at 872°C is observed also (Figure 1b).

The second binary sulfide Cu-Cu<sub>2</sub>S (B-R2) subsystem is characterized by the liquid immiscibility region mkn and the monotectic L1→L2+Cu<sub>2</sub>S (m(n): L1→L2+R2) at 1105°C and eutectic L→Cu+Cu<sub>2</sub>S (e<sub>BR2</sub>: L→B+R2) reactions (Figure 1c).

High-temperature part of the quasi-binary section CoS-Cu<sub>2</sub>S (R1-R2) constructed experimentally [18] shows the eutectic equilibrium L→CoS+Cu<sub>2</sub>S (e<sub>R1R2</sub>: L→R1+R2) at 941°C (Figure 1d).

The ternary Co-Cu-CoS-Cu<sub>2</sub>S (A-B-R1-R2) subsystem is characterized by the wide region of liquid-phase immiscibility (Figure 2). The critical point K of the immiscibility region has the temperature 1334°C. Tie-lines (K is their degeneration) on the border of the immiscibility region are isotherms which form two ruled surfaces as the boundaries of three-phase monotectic reactions with participation of either Co (L1→L2+Co and directing lines KN and KM) or the solid solution on the base of Cu<sub>2</sub>S (L1→L2+Cu<sub>2</sub>S and directing lines nN and mM). The thermal analysis showed the temperature 1076°C of the four-phase invariant monotectic transformation L1→L2+Co+Cu<sub>2</sub>S (M(N): L1→L2+A+R2) [18]. Besides, the subsystem includes two invariant transformations of quasi-

peritectic type L+CoS→Cu<sub>2</sub>S+Co<sub>4</sub>S<sub>3</sub> (Q<sub>1</sub>: L+R1→R2+R3) at 875°C, L+Co→Cu+Cu<sub>2</sub>S (Q<sub>2</sub>: L+A→B+R2) at 1070°C, and one invariant transformation of the eutectic type L→Co+Cu<sub>2</sub>S+Co<sub>4</sub>S<sub>3</sub> (E: L→A+R2+R3) at 837±2°C. Since the reaction Q<sub>2</sub> temperature is not experimentally determined and is indicated only in the temperature interval 1067-1076°C [18], which is accepted as equal to 1070°C in the 3D model.

Concentration coordinates of the apexes of complexes which correspond to quasi-peritectic Q<sub>1</sub> and Q<sub>2</sub> reactions are cited in [18] such that the points Q<sub>1</sub> and Q<sub>2</sub>, corresponding to liquid concentrations occur within R<sub>1Q1</sub>R<sub>2Q1</sub>R<sub>3Q1</sub> and A<sub>Q2</sub>B<sub>Q2</sub>R<sub>2Q2</sub> triangles, and they correspond not to quasi-peritectic Q<sub>1</sub>: L+R1→R2+R3 and Q<sub>2</sub>: L+A→B+R2 reactions but to eutectic L→R1+R2+R3 and L→A+B+R2+R3 ones, accordingly. Therefore, for the 3D computer model coordinates of the R<sub>3Q1</sub> and B<sub>Q2</sub> points were corrected in such a way that the Q<sub>1</sub> and Q<sub>2</sub> points would not appear inside the tie-triangle (Table 1).

### 3. 3D simulation

3D simulation was carried out in several steps [31]. The scheme of uni- and invariant states (Table 2) was formed firstly. It is the description of uni- and invariant reactions and, correspondingly, of three- and

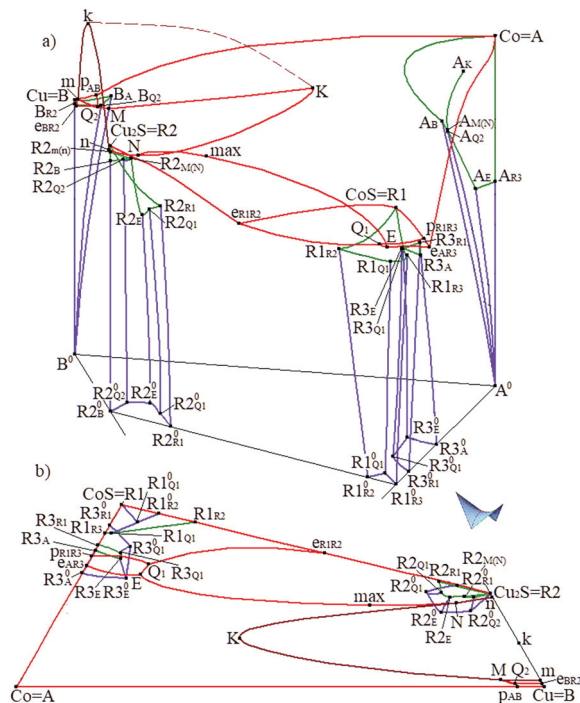


Figure 2. 3D computer model of the subsystem Co-Cu-CoS-Cu<sub>2</sub>S (A-B-R1-R2) T-x-y diagram (a) and its x-y projection (b) (3D computer model is constructed down to 800°C (corresponding points below the ternary eutectic E temperature 837°C are noted by the superscript “0”))



**Table 1.** Base points (weight portions), according to which the 3D model of the subsystem Co-Cu-CoS-Cu<sub>2</sub>S (A-B-R1-R2) has been designed <sup>a</sup>

No	Point	z <sub>1</sub> (Co)	z <sub>2</sub> (S)	z <sub>3</sub> (Cu)	T°C	No	Point	z <sub>1</sub> (Co)	z <sub>2</sub> (S)	z <sub>3</sub> (Cu)	T°C
1	Co (A)	1	0	0	1495	32	<b>m</b>	0	0.015	0.985	1105
2	Cu (B)	0	0	1	1084.6	33	<b>n</b>	0	0.197	0.803	1105
3	CoS (R1)	0.625	0.375	0	1182	34	R2 <sub>m(n)</sub>	0	0.205	0.795	1105
4	Cu <sub>2</sub> S (R2)	0	0.205	0.795	1131	35	<b>k</b>	0	0.088	0.912	1510
5	<b>p</b> <sub>AB</sub>	0.051	0	0.959	1112	36	<b>e</b> <sub>R1R2</sub>	0.270	0.293	0.437	941
6	A <sub>B</sub>	0.873	0	0.127	1112	37	R1 <sub>R2</sub>	0.480	0.361	0.159	941
7	B <sub>A</sub>	0.086	0	0.914	1112	38	R2 <sub>R1</sub>	0.084	0.232	0.684	941
8	<b>e</b> <sub>AR3</sub>	0.734	0.266	0	872	39	<b>e</b> <sub>BR2</sub>	0	0.0077	0.9923	1067
9	A <sub>R3</sub>	1	0	0	872	40	B <sub>R2</sub>	0	0	1	1067
10	R3 <sub>A</sub>	0.701	0.299	0	872	41	R2 <sub>B</sub>	0	0.205	0.795	1067
11	<b>P</b> <sub>R1R3</sub>	0.714	0.286	0	930	42	<b>M</b>	0.074	0.016	0.910	1076
12	R1 <sub>R3</sub>	0.645	0.355	0	930	43	<b>N</b>	0.074	0.185	0.741	1076
13	R3 <sub>R1</sub>	0.698	0.302	0	930	44	<b>K</b>	0.523	0.106	0.371	1334
14	<b>Q</b> <sub>1</sub>	0.614	0.270	0.116	875	45	<b>Q</b> <sub>2</sub>	0.052	0.007	0.951	1070
15	R1 <sub>Q1</sub>	0.653	0.337	0.010	875	46	A <sub>Q2</sub>	0.887	0	0.113	1070
16	R2 <sub>Q1</sub>	0.092	0.207	0.701	875	47	B <sub>Q2</sub> <sup>b</sup>	0.062 (0.035)	0	0.938 (0.965)	1070
17	R3 <sub>Q1</sub> <sup>b</sup>	0.661 (0.668)	0.282 (0.263)	0.057 (0.069)	875	48	R2 <sub>Q2</sub>	0.035	0.197	0.768	1070
18	<b>E</b>	0.642	0.246	0.112	837	49	A <sub>M(N)</sub>	0.887	0	0.113	1076
19	A <sub>E</sub>	0.934	0	0.066	837	50	R2 <sub>M(N)</sub>	0.052	0.199	0.749	1076
20	R2 <sub>E</sub>	0.080	0.196	0.724	837	51	A <sub>K</sub>	0.924	0	0.076	1334
21	R3 <sub>E</sub>	0.668	0.263	0.069	837	52	<b>max</b>	0.240	0.180	0.580	1091
22	R1 <sup>0</sup> <sub>Q1</sub>	0.590	0.361	0.049	800	53	A <sup>0</sup> <sub>Q2</sub>	1	0	0	800
23	R2 <sup>0</sup> <sub>Q1</sub>	0.119	0.208	0.673	800	54	B <sup>0</sup> <sub>Q2</sub>	0	0	1	800
24	R3 <sup>0</sup> <sub>Q1</sub>	0.631	0.307	0.062	800	55	R2 <sup>0</sup> <sub>Q2</sub>	0.560	0.167	0.273	800
25	A <sup>0</sup> <sub>B</sub>	1	0	0	800	56	A <sup>0</sup> <sub>R3</sub>	1	0	0	800
26	B <sup>0</sup> <sub>A</sub>	0	0	1	800	57	R3 <sup>0</sup> <sub>A</sub>	0.750	0.250	0	800
27	B <sup>0</sup> <sub>R2</sub>	0	0	1	800	58	R1 <sup>0</sup> <sub>R2</sub>	0.540	0.381	0.079	800
28	R2 <sup>0</sup> <sub>B</sub>	0	0.205	0.795	800	59	R2 <sup>0</sup> <sub>R1</sub>	0.005	0.264	0.731	800
29	A <sup>0</sup> <sub>E</sub>	1	0	0	800	60	R1 <sup>0</sup> <sub>R3</sub>	0.600	0.400	0	800
30	R2 <sup>0</sup> <sub>E</sub>	0.113	0.163	0.724	800	61	R3 <sup>0</sup> <sub>R1</sub>	0.645	0.355	0	800
31	R3 <sup>0</sup> <sub>E</sub>	0.666	0.249	0.085	800						

<sup>a</sup> The lowest temperatures here is 800°C (below the eutectic invariant point E at 837°C); 3D model is constructed down to this temperature and corresponding points are noted by the superscript "0"

<sup>b</sup> Concentration coordinates of the R3<sub>Q1</sub> and B<sub>Q2</sub> points were corrected in such a way that the Q1 and Q2 points would not fall inside the R1<sub>Q1</sub>R2<sub>Q1</sub>R3<sub>Q1</sub> and A<sub>Q2</sub>B<sub>Q2</sub>R2<sub>Q2</sub> tie-triangles, accordingly. Coordinates of R3<sub>Q1</sub> and B<sub>Q2</sub> points, which correspond to data [18], are indicated in the brackets

four-phase regions (degenerated into a planar complex).

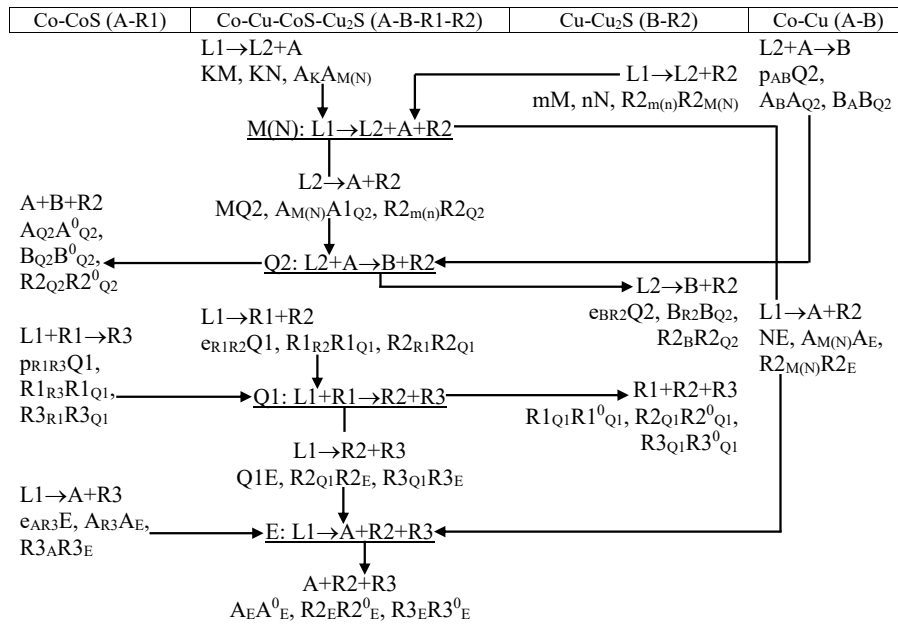
Further, it was transformed into the three-dimensional form, in which the corresponding ruled surfaces and the isothermal planes, which play the role of the complexes and correspond to invariant reactions, were graphically presented. Then the necessary unruled surfaces (*q* - liquidus, *s* - solidus, *v* - solvus, etc in the 3D model and in the Table 3) were

added to these ruled surfaces and planes.

As a result, the prototype of T-x-y diagram was obtained, which was transformed into the real system T-x-y diagram 3D model after the input of the coordinates of all base points and correction of the curvature of lines and surfaces (Figure 2). It is possible to divide the 3D image of the T-x-y diagram (Figure 2) into its constituent ("exploded" [23]) phase regions (Figure 3; Figure 4).



**Table 2.** Scheme of uni- and invariant states of the subsystem Co-Cu-CoS-Cu<sub>2</sub>S (A-B-R1-R2) (Figure 2)<sup>a</sup>,  $k > A > K > R1 > R2 > p_{AB} > m(n) > B > M(N) > Q2 > e_{BR2} > e_{R1R2} > p_{R1R3} > e_{AR3} > Q1 > E$ <sup>b</sup>



<sup>a</sup> The lowest temperatures here is 800°C (below the eutectic invariant point E at 837°C); 3D model is constructed down to this temperature and corresponding points are noted by the superscript "0"

<sup>b</sup> Co (A), Cu (B), CoS (R1), Cu<sub>2</sub>S (R2), Co<sub>3</sub>S<sub>3</sub> (R3)

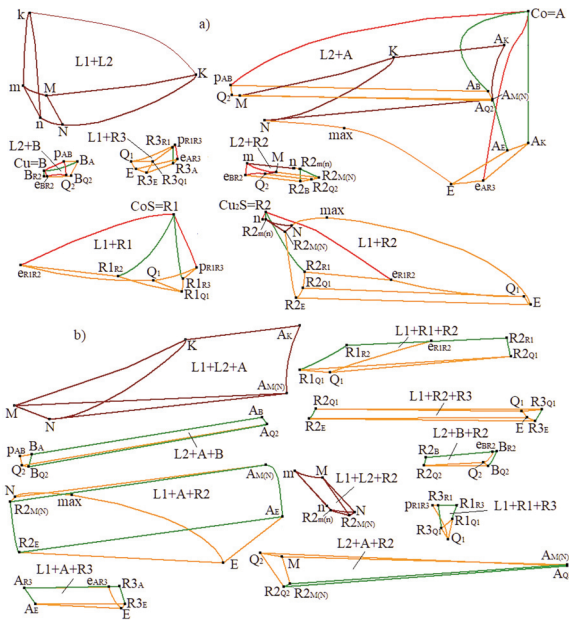


**Figure 3.** Phase regions with the melt (L) of the subsystem Co-Cu-CoS-Cu<sub>2</sub>S (A-B-R1-R2) T-x-y diagram: two-phase (a) and three-phase regions (b)

So, the Co-Cu-CoS-Cu<sub>2</sub>S (A-B-R1-R2) subsystem T-x-y diagram 3D model (Figure 5a; Figure 6a) is well agreed with the experimental data in the liquidus (Figure 5b) and solidus (Figure 6b) surfaces, correspondingly. Therefore it can be considered as the qualitative generalization of experimental data and be used as the basis for the further study of the system.

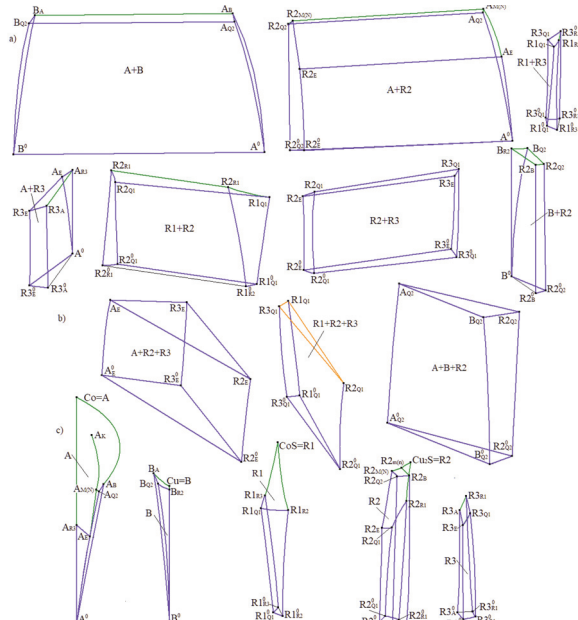


**Figure 4.** Phase regions without the melt (L) of the subsystem Co-Cu-CoS-Cu<sub>2</sub>S (A-B-R1-R2) T-x-y diagram: two-phase (a), three-phase (b) & one-phase (c)

The analysis of the T-x-y diagram geometric structure is presented as the scheme of uni- and invariant states (Table 2). Four M(N), Q<sub>2</sub>, Q<sub>1</sub>, and E invariant transformations of the Co-Cu-CoS-Cu<sub>2</sub>S (A-B-R1-R2) subsystem, in accordance with the temperature row, are



written to the scheme, where every three-phase reaction has the initial and final points of the interacting phases concentrations. The contours of the unruled surfaces are combined from these lines. For example,  $e_{R_1R_2}Q_1$ ,  $R_1R_2R_1Q_1$ ,  $R_2R_1R_2Q_1$  lines correspond to the concentrations change in the liquid (L) and solid (R1 and R2) phases in the  $L \rightarrow R_1 + R_2$  reaction.

The  $e_{R_1R_2}Q_1$  curve is one of the contour lines of CoS (R1) on the border of two liquidus surfaces, while the  $R_1R_2R_1Q_1$  curve forms its solidus contour. The  $R_2R_1R_2Q_1$  curve participates in the shaping of R2 solidus contour. Thus, the scheme makes it possible to determine the types (ruled, unruled, plane, etc.) and to calculate the number of all surfaces, to indicate their contours, and to describe the borders of all phase regions. As a result, the Co-Cu-CoS-Cu<sub>2</sub>S T-x-y diagram consists of 82 surfaces (Table 3) and 33 phase regions (Table 4; Figure 3; Figure 4).

The 3D model was constructed on the basis of experimental liquidus and solidus surfaces. It consists of the immiscibility cupola, six liquidus and six solidus surfaces of Co (A), Cu (B), CoS (R1), Cu<sub>2</sub>S (R2), Co<sub>4</sub>S<sub>3</sub> (R3) (where the liquidus and solidus surfaces of Cu<sub>2</sub>S (R2) are more complex; both surfaces are divided into two parts – “up” and “down” ( $q_{R_2, up}$ ,  $q_{R_2, down}$ ,  $s_{R_2, up}$ ,  $s_{R_2, down}$  in Table 3).

Earlier, the reference book of computer models of T-x-y and T-x-y-z diagrams of the basic topological types was created [35]. It includes >200 3D models of T-x-y and 7 4D models of T-x-y-z diagrams. Each computer model is the prototype of the phase diagram with corresponding topology. In the case of the Co-Cu-CoS-Cu<sub>2</sub>S T-x-y diagram the construction of its 3D model incorporates the templates of the system with the binary incongruently melting compound and of the system with the univariant monotectic immiscibility.

In contrast to the simple surfaces of the primary crystallization of copper and R1, R3, the liquidus surface of Co (A) has a complicated contour. It is formed by eight points A,  $e_{AR_3}$ , E, N, K, M, Q<sub>2</sub>,  $p_{AB}$  (the point “max” denotes the curvature of the NE line and it is not considered in this case as the liquidus surface contour) (Figure 2b).

Since the contour of the Co (A) liquidus is formed by eight points, the solidus corresponding to it must be given by eight points. However, there are only seven: A,  $A_{R_3}$ ,  $A_E$ ,  $A_K$ ,  $A_{M(N)}$ ,  $A_{Q_2}$ ,  $A_B$ . Therefore, the basic innovation in this type of computer models consists of the presence of the  $A_K A_{M(N)}$  pseudo-fold on this surface of solidus [28-30]. It is the directing curve of two ruled surfaces and it does not influence the smoothness of the Co (A) solidus surface. Its upper  $A_K$  point has the critical K point temperature in the intersection of the immiscibility cupola with this liquidus surface. Thanks to the fold, the liquidus and solidus become topologically equivalent surfaces, because the  $A_K A_{M(N)}$  curve is the conjugate one with two parts of the arc NKM.

Because of the liquid immiscibility to L1 and L2 under the cupola which intersects the Q2E line of co-crystallization of A and R2 crystals, it is necessary in this, would seem routine, work to distinguish what precisely liquid, L1 or L2, the Co (A), Cu (B), Cu<sub>2</sub>S (R2) crystals coexist with. Since the monotectic reaction in the binary Cu-Cu<sub>2</sub>S (B-R2) subsystem is carried out in the form  $L1 \rightarrow L2 + R2$ , then it must be the two-phase region  $L2 + R2$  in the lower part (between the mM and  $p_{AB}Q_2$  lines under the  $q_{R_2, up}$  liquidus surface) and  $L1 + R2$  region (under the  $q_{R_2, down}$  liquidus surface) in the upper part of the Co-Cu-CoS-Cu<sub>2</sub>S (A-B-R1-R2) subsystem. Corresponding surfaces of liquidus and solidus (borders of Cu<sub>2</sub>S (R2)) primary crystallization beginning and finishing) are also divided into two parts.

Besides the immiscibility cupola, six liquidus and six solidus surfaces, the T-x-y diagram, includes 39 ruled surfaces and 16 planes (simplexes of four complexes), corresponding to Q1, Q2, M(N) and E reactions.

The ruled surfaces with KN, KM,  $A_K A_{M(N)}$  and nN, mM,  $R_2^{m(n)} R_2^{M(N)}$  directing curves, respectively, serve as boundaries of the three-phase regions  $L1 + L2 + A$  and  $L1 + L2 + R2$ . The group of five three-phase regions includes liquid L1 ( $L1 + A + R2$ ,  $L1 + A + R3$ ,  $L1 + R1 + R2$ ,  $L1 + R1 + R3$ ,  $L1 + R2 + R3$ ) and the group of three three-phase regions includes liquid L2 ( $L2 + A + B$ ,  $L2 + A + R2$ ,  $L2 + B + R2$ ). Liquidus NE,  $e_{AR_3}E$ ,  $e_{R_1R_2}Q_1$ ,  $p_{R_1R_3}Q_1$ , Q1E, и  $p_{AB}Q_2$ , MQ2,  $e_{BR_2}Q_2$  curves are, in particular, the directing lines of ruled surfaces, which serve as boundaries of these regions. Other three three-phase regions are formed in the sub-solidus:  $R1 + R2 + R3$ ,  $A + B + R2$ ,  $A + R2 + R3$  below, correspondingly, Q<sub>1</sub>, Q<sub>2</sub>, E planes.

The T-x-y diagram is examined in this paper from the highest 1510°C temperature down to 800°C. This boundary for the 3D model is selected conditionally in order to show only all phase transformations with the participation of liquid, and also phase transformations in the subsolidus, connected with the Q1, Q2, E invariant reactions. Therefore, there are only 14 solvus surfaces in the temperature interval 837-800°C (Table 3).

After the transformation of the scheme of uni- and invariant states from the tabular form into the graphic one, when the horizontal (isothermal) planes corresponding to the M(N), Q1, Q2, E invariant reactions and the ruled surfaces are designed, the T-x-y diagram prototype is obtained. It is converted into the real system T-x-y diagram 3D model, when concentrations and temperatures of base points (Table 1) are introduced, and the curvature of lines and surfaces is specified. Comparison of the 3D model (Figure 5a) and experimental [18] (Figure 5b) isothermal lines on the liquidus surfaces shows that the model line 1335°C adjoins the critical point K, and this is correct, because the temperature of this point is equal to 1334°C; however, experimental line passes far from this point K.

There are considerable disagreements according to



Table 3. Surfaces of the T-x-y diagram

No	Designation	Contour	No	Designation	Contour
<b>liquidus - q</b>					
1	$q_A$	$Ae_{AR3} E_{max} N_{KM} Q_2 p_{AB}$	4	$q_{R2\_up}$	$R_2 n N_{max} E_{Q1} e_{R1R2}$
2	$q_B$	$B p_{AB} Q_2 e_{BR2}$	5	$q_{R2\_down}$	$e_{BR2} Q_2 M m$
3	$q_{R1}$	$R_1 e_{R1R2} Q_1 p_{R1R3}$	6	$q_{R3}$	$e_{AR3} p_{R1R3} Q_1 E$
7		Immiscibility cupola		i	nNKMmk
<b>solidus - s</b>					
8	$s_A^a$	$AA_{R3} A_E A_{M(N)} A_K A_{Q2} A_B$	11	$s_{R2\_up}$	$R_2 R_2_{m(n)} R_2_{M(N)} R_2 E R_2 Q_1 R_2 R_1$
9	$s_B^a$	$BB_A B_{Q2} B_{R2}$	12	$s_{R2\_down}$	$R_2 B R_2 Q_2 R_2_{M(N)} R_2_{m(n)}$
10	$s_{R1}$	$R_1 R_1 R_2 R_1 Q_1 R_1 R_3$	13	$s_{R3}$	$R_3 A R_3 R_3 Q_1 R_3 E$
<b>solvus - v</b>					
14	$v_{AB}^a$	$A_B A^0 B A^0 Q_2 A_{Q2}$	21	$v_{BA}^a$	$B_A B^0 A B^0 Q_2 B_{Q2}$
15	$v_{AR2}$	$A_{Q2} A^0 Q_2 A^0 E A_E A_{M(N)}$	22	$v_{R2A}$	$R_2 Q_2 R_2^0 Q_2 R_2^0 E R_2 R_2_{M(N)}$
16	$v_{AR3}^a$	$A_{R3} A^0 R_3 A^0 A_E$	23	$v_{R3A}$	$R_3 A R_3^0 A R_3^0 R_3 E$
17	$v_{BR2}^a$	$B_{R2} B^0 R_2 B^0 Q_2 B_{Q2}$	24	$v_{R2B}$	$R_2 B R_2^0 B R_2^0 Q_2 R_2 Q_2$
18	$v_{R1R2}$	$R_1 Q_1 R_1^0 Q_1 R_1^0 R_2 R_1 R_2$	25	$v_{R2R1}$	$R_2 Q_1 R_2^0 Q_1 R_2^0 R_1 R_2 R_1$
19	$v_{R1R3}$	$R_1 R_3 R_1^0 R_3 R_1^0 Q_1 R_1 Q_1$	26	$v_{R3R1}$	$R_3 R_1 R_3^0 R_1 R_3^0 Q_1 R_3 Q_1$
20	$v_{R2R3}$	$R_2 R_2^0 R_2^0 Q_1 R_2 Q_1$	27	$v_{R3R2}$	$R_3 E R_3^0 E R_3^0 Q_1 R_3 Q_1$
<b>ruled surfaces - r (types of q, s, v, i [31])</b>					
28	$q_{AB}^r$	$p_{AB} Q_2 A_{Q2} A_B$	49	$q_{BR2}^r$	$e_{BR2} Q_2 B_{Q2} B_{R2}$
29	$q_{BA}^r$	$p_{AB} Q_2 B_{Q2} B_A$	50	$q_{R2B}^r$	$e_{BR2} Q_2 R_2 Q_2 R_2 B$
30	$s_{AB}^r$	$A_B A_{Q2} B_{Q2} B_A$	51	$s_{BR2}^r$	$B_{R2} B_{Q2} R_2 Q_2 R_2 B$
31	$q_{AR2\_up}^r$	$N_{max} E A_E A_{M(N)}$	52	$q_{R1R2}^r$	$e_{R1R2} Q_1 R_1 Q_1 R_1 R_2$
32	$q_{R2A\_up}^r$	$N_{max} E R_2 R_2_{M(N)}$	53	$q_{R2R1}^r$	$e_{R1R2} Q_1 R_2 Q_1 R_2 R_1$
33	$s_{AR2\_up}^r$	$A_E A_{M(N)} R_2_{M(N)} R_2 E$	54	$s_{R1R2}^r$	$R_1 R_2 R_1 Q_1 R_2 Q_1 R_2 R_1$
34	$q_{AR2\_down}^r$	$MQ_2 A_{Q2} A_{M(N)}$	55	$q_{R1R3}^r$	$p_{R1R3} Q_1 R_1 Q_1 R_1 R_3$
35	$q_{R2A\_down}^r$	$MQ_2 R_2 Q_2 R_2_{M(N)}$	56	$q_{R3R1}^r$	$p_{R1R3} Q_1 R_3 Q_1 R_3 R_1$
36	$s_{AR2\_down}^r$	$A_{Q2} A_{M(N)} R_2_{M(N)} R_2 Q_2$	57	$s_{R1R3}^r$	$R_1 R_3 R_1 Q_1 R_3 Q_1 R_3 R_1$
37	$q_{AR3}^r$	$e_{AR3} E A_E A_{R3}$	58	$q_{R2R3}^r$	$Q_1 E R_2 E R_2 Q_1$
38	$q_{R3A}^r$	$e_{AR3} E R_3 R_3 E$	59	$q_{R3R2}^r$	$Q_1 E R_3 E R_3 Q_1$
39	$s_{AR3}^r$	$A_{R3} A_E R_3 R_3 A$	60	$s_{R2R3}^r$	$R_2 Q_1 R_2 E R_3 E R_3 Q_1$
40	$i_{MNK}^r$	MNK	61	$i_{MR2}^r$	$m M R_2 R_2_{M(N)} R_2_{m(n)}$
41	$i_{AM}^r$	$M K A_K A_{M(N)}$	62	$i_{NR2}^r$	$n N R_2 R_2_{M(N)} R_2_{m(n)}$
42	$i_{AN}^r$	$N K A_K A_{M(N)}$	63	$i_{MN}^r$	mMNn
43	$v_{R1R2(Q1)}^r$	$R_1 Q_1 R_1^0 Q_1 R_2^0 Q_1 R_2 Q_1$	64	$v_{AB(Q2)}^r$	$A_{Q2} A^0 Q_2 B^0 Q_2 B_{Q2}$
44	$v_{R1R3(Q1)}^r$	$R_1 Q_1 R_1^0 Q_1 R_3^0 Q_1 R_3 Q_1$	65	$v_{AR2(Q2)}^r$	$A_{Q2} A^0 Q_2 R_2^0 Q_2 R_2 Q_2$
45	$v_{R2R3(Q1)}^r$	$R_2 Q_1 R_2^0 Q_1 R_3^0 Q_1 R_3 Q_1$	66	$v_{BR2(Q2)}^r$	$B_{Q2} B^0 Q_2 R_2^0 Q_2 R_2 Q_2$
46	$v_{AR2(E)}^r$	$A_E A_E^0 R_2^0 E R_2 E$			
47	$v_{AR3(E)}^r$	$A_E A_E^0 R_3^0 E R_3 E$			
48	$v_{R2R3(E)}^r$	$R_2 E R_2^0 E R_3^0 E R_3 E$			
<b>horizontal complexes - h</b>					
67	$h_{R1R2R3}^{Q1}$	$R_1 Q_1 R_2 Q_1 R_3 Q_1$	75	$h_{ABR2}^{Q2}$	$A_{Q2} B_{Q2} R_2 Q_2$
68	$h_{R1R2Q1}$	$R_1 Q_1 R_2 Q_1 Q_1$	76	$h_{ABQ2}$	$A_{Q2} B_{Q2} Q_2$
69	$h_{R1R3Q1}$	$R_1 Q_1 R_3 Q_1 Q_1$	77	$h_{AR2Q2}$	$A_{Q2} R_2 Q_2 Q_2$
70	$h_{R2R3Q1}$	$R_2 Q_1 R_3 Q_1 Q_1$	78	$h_{BR2Q2}$	$B_{Q2} R_2 Q_2 Q_2$
71	$h_{AR2R3}^E$	$A_E R_2 R_3 E$	79	$h_{AR2M}$	$A_{M(N)} R_2_{M(N)} M$
73	$h_{AR2E}$	$A_E R_2 E$	80	$h_{AR2N}$	$A_{M(N)} R_2_{M(N)} N$
73	$h_{AR3E}$	$A_E R_3 E$	81	$h_{AMN}$	$A_{M(N)} MN$
74	$h_{R2R3E}$	$R_2 E R_3 E$	82	$h_{R2MN}$	$R_2_{M(N)} MN$

<sup>a</sup> The  $s_A, s_B$  surfaces of solidus and  $v_{AB}, v_{BA}, v_{AR3}, v_{BR2\_down}$  surfaces of solvus merge into the Co-Cu (A-B) face of the prism because of the degeneration of the solidus and solvus lines in the binary subsystems Co-CoS (A-R1) and Cu-Cu<sub>3</sub>S (B-R2) ( $A_{R3}$  and  $B_{R2}$  points have such concentration coordinates that they fall into the A and B apices, respectively), and also because of the concentration coordinates of  $A_{Q2}, A_E, B_{Q2}$  points (Table 1), which fall on the Co-Cu (A-B) face (Figure 2)



Table 4. Phase regions (Figure 3; Figure 4)

No	Region	Boundary surfaces	Adjacent phase regions
1	L1+L2	$i, i_{MNK}^r, i_{MN}^r$	L1+L2+A, L1+L2+R2
2	L1+A	$q_A, s_A, q_{AR2\_up}^r, q_{AR3}^r, i_{AN}^r$	L1, A, L1+L2+A, L1+A+R2, L1+A+R3
3	L2+A	$q_A, s_A, q_{AR2\_down}^r, i_{AM}^r, q_{AB}^r$	L2, A, L1+L2+A, L2+A+R2, L2+A+B
4	L2+B	$q_B, s_B, q_{BA}^r, q_{BR2}^r$	L2, B, L+A+B, L+B+R2
5	L1+R1	$q_{R1}, s_{R1}, q_{R1R2}^r, q_{R1R3}^r$	L1, R1, L1+R1+R2, L1+R1+R3
6	L1+R2	$q_{R2\_up}^r, s_{R2\_up}^r, q_{R2A\_up}^r, q_{R2R1}^r, q_{R2R3}^r, i_{NR2}^r$	L1, R2, L1+A+R2, L1+R1+R2, L1+R2+R3, L1+L2+R2
7	L2+R2	$q_{R2\_down}^r, s_{R2\_down}^r, q_{R2A\_down}^r, q_{R2B}^r, i_{MR2}^r$	L2, R2, L2+A+R2, L2+B+R2, L1+L2+R2
8	L1+R3	$q_{R3}, s_{R3}, q_{R3A}^r, q_{R3R1}^r, q_{R3R2}^r$	L1, R3, L1+A+R3, L1+R1+R3, L1+R2+R3
9	A	$s_A, v_{AB}, v_{AR2}, v_{AR3}$	L1+A (L2+A), A+B, A+R2, A+R3
10	B	$s_B, v_{BA}, v_{BR2}$	L2+B, A+B, B+R2
11	R1	$s_{R1}, v_{R1R2}, v_{R1R3}$	L1+R1, R1+R2, R1+R3
12	R2	$s_{R2\_up}, s_{R2\_down}, v_{R2A}, v_{R2R1}, v_{R2R3}, v_{R2B}$	L1+R2, L2+R2, A+R2, R1+R2, R2+R3, B+R2
13	R3	$s_{R3}, v_{R3A}, v_{R3R1}, v_{R3R2}$	L1+R3, A+R3, R1+R3, R2+R3
14	L1+L2+A	$i_{MNK}^r, i_{AM}^r, i_{AN}^r, h_{AMN}$	L1+L2, L1+A, L2+A, L1+L2+A+R2
15	L1+L2+R2	$i_{MN}^r, i_{MR2}^r, i_{NR2}^r, h_{R2MN}$	L1+L2, L1+R2, L2+R2, L1+L2+A+R2
16	L2+A+B	$q_{AB}^r, q_{BA}^r, s_{AB}^r, h_{ABQ2}$	L2+A, L2+B, A+B, L2+A+B+R2
17	L1+A+R2	$q_{AR2\_up}^r, q_{R2A\_up}^r, s_{AR2\_up}^r, h_{AR2E}$	L1+A, L1+R2, A+R2, L1+A+R2+R3
18	L2+A+R2	$q_{AR2\_down}^r, q_{R2A\_down}^r, s_{AR2\_down}^r, h_{AR2Q2}$	L2+A, L2+R2, A+R2, L2+A+B+R2
19	L1+A+R3	$q_{AR3}^r, q_{R3A}^r, s_{AR3}^r, h_{AR3E}$	L1+A, L1+R3, A+R3, L1+A+R2+R3
20	L2+B+R2	$q_{BR2}^r, q_{R2B}^r, s_{BR2}^r, h_{BR2Q2}$	L2+B, L2+R2, B+R2, L2+A+B+R2
21	L1+R1+R2	$q_{R1R2}^r, q_{R2R1}^r, s_{R1R2}^r, h_{R1R2Q1}$	L1+R1, L1+R2, R1+R2, L1+R1+R2+R3
22	L1+R1+R3	$q_{R1R3}^r, q_{R3R1}^r, s_{R1R3}^r, h_{R1R3Q1}$	L1+R1, L1+R3, R1+R3, L1+R1+R2+R3
23	L1+R2+R3	$q_{R2R3}^r, q_{R3R2}^r, s_{R2R3}^r, h_{R2R3Q1}, h_{R2R3E}$	L1+R2, L1+R3, R2+R3, L1+R1+R2+R3, L1+A+R2+R3
24	A+B	$v_{AB}, v_{BA}, s_{AB}^r, v_{AB(Q2)}^r$	A, B, L+A+B, A+B+R2, L2+A+B+R2
25	A+R2	$v_{AR2}, v_{R2A}, s_{AR2\_up}^r, s_{AR2\_down}^r, v_{AR2(E)}^r, v_{AR2(Q2)}^r, h_{AR2E}, h_{AR2N}, h_{AR2M}, h_{AR2Q2}$	A, R2, L1+A+R2, L2+A+R2, A+R2+R3, A+B+R2, L1+A+R2+R3, L1+L2+A+R2, L2+A+B+R2
26	A+R3	$v_{AR3}, v_{R3A}, s_{AR3}^r, v_{AR3(E)}^r$	A, R3, L1+A+R3, A+R2+R3, L1+A+R2+R3
27	B+R2	$v_{BR2}, v_{R2B}, s_{BR2}^r, v_{BR2(Q2)}^r$	B, R2, L2+B+R2, A+B+R2, L2+A+B+R2
28	R1+R2	$v_{R1R2}, v_{R2R1}, s_{R1R2}^r, v_{R1R2(Q1)}^r$	R1, R2, L1+R1+R2, R1+R2+R3, L1+R1+R2+R3
29	R1+R3	$v_{R1R3}, v_{R3R1}, s_{R1R3}^r, v_{R1R3(Q1)}^r$	R1, R3, L1+R1+R3, R1+R2+R3, L1+R1+R2+R3
30	R2+R3	$v_{R2R3}, v_{R3R2}, s_{R2R3}^r, v_{R2R3(Q1)}, v_{R2R3(E)}^r$	R2, R3, L1+R2+R3, R1+R2+R3, L1+R1+R2+R3, A+R2+R3, L1+A+R2+R3
31	A+B+R2	$v_{AB(Q2)}^r, v_{AR2(Q2)}^r, v_{BR2(Q2)}^r, h_{ABR2}^{Q2}$	A+B, A+R2, B+R2, L2+A+B+R2
32	A+R2+R3	$v_{AR2(E)}^r, v_{AR3(E)}^r, v_{R2R3(E)}^r, h_{AR2R3}^E$	A+R2, A+R3, R2+R3, L1+A+R2+R3
33	R1+R2+R3	$v_{R1R2(Q1)}^r, v_{R1R3(Q1)}^r, v_{R2R3(Q1)}^r, h_{R1R2R3}^{Q1}$	R1+R2, R1+R3, R2+R3, L1+R1+R2+R3



the form of the isothermal line 1080°C on the liquidus surface of  $\text{Cu}_2\text{S}$  (R2). The 3D model of this surface includes two lines at 1080°C. The first one is located around the N point, since the temperature of the N point is equal to 1076°C (Figure 5a). The second line at 1080°C is located between the NmaxE (in the temperature interval of 1076-1091-837°C) and  $\text{Cu}_2\text{S-e}_{\text{RIR2}}$  (1131-941°C) lines. As for the experimental version, the isothermal line (1080°C) is located around the point of maximum with 1091°C (Figure 5b). But, it is impossible as the temperature 1080°C is on the  $\text{Cu}_2\text{S-e}_{\text{RIR2}}$  line.

The main difference between the 3D model (Figure 6a) and the experimental version (Figure 6b) isothermal lines of the solidus surfaces and ruled surfaces connected

with them is caused by the already above discussed contradictions in the concentration coordinates of the apexes of the complexes, which correspond to the Q1 and Q2 quasi-peritectic reactions (Table 1).

As a whole, it is possible to consider that the 3D computer model adequately reproduces the experiment, and therefore, it can be used in the practical work; in particular, for designing any isopleths. For instance, two isopleths were designed: parallel to the sides Co-Cu (A-B)  $\text{S}_1(0.85, 0.15, 0)$ - $\text{S}_2(0, 0.15, 0.85)$  (Figure 7a) and CoS-Cu (R1-B) (Figure 7b). Three-phase regions  $\text{L1+L2+R2}$ ,  $\text{L2+A+R2}$ ,  $\text{L2+B+R2}$  in these sections merge in the line because of the close arrangement of points and small temperature differences in the angle of copper.

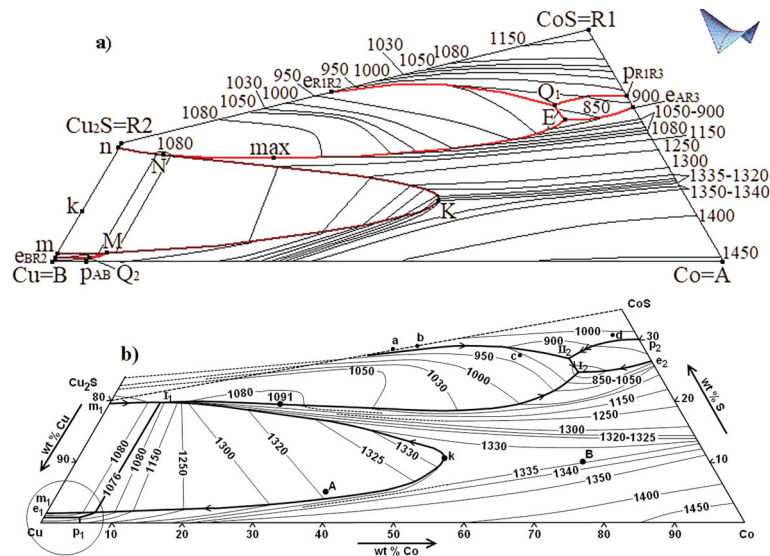


Figure 5. Liquidus surfaces of the subsystem  $\text{Co-Cu-CoS-Cu}_2\text{S}$  (A-B-R1-R2) (the ruled surfaces with nN-mM and NK-MK directing curves are shown within the cupola): 3D model (a), experimental [18] (b)

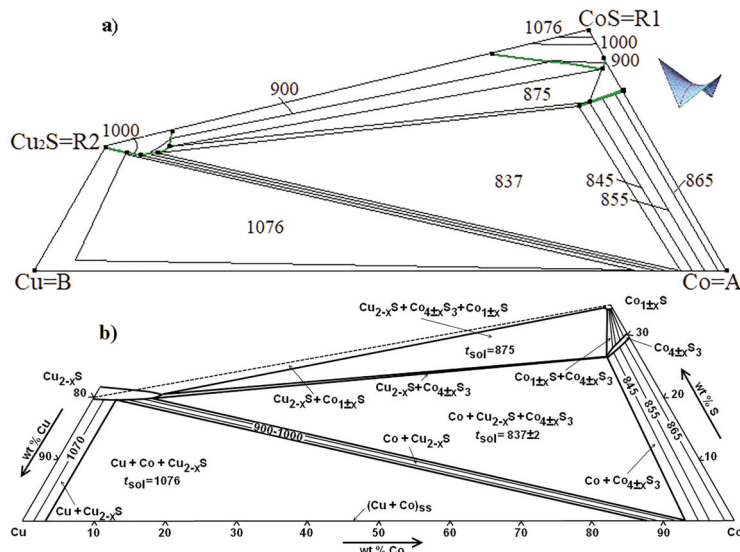
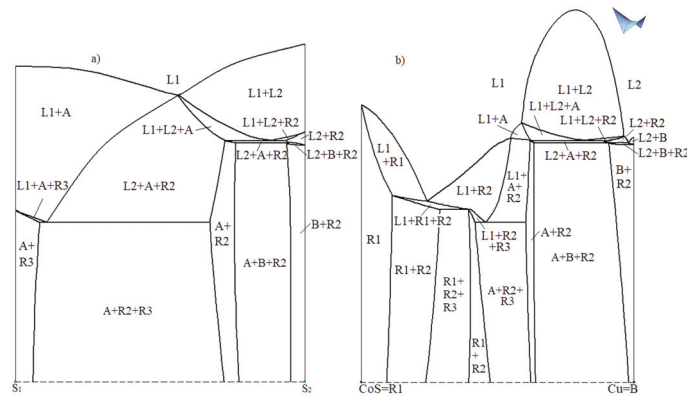


Figure 6. Surfaces of solidus and adjoining it ruled surfaces of the subsystem  $\text{Co-Cu-CoS-Cu}_2\text{S}$  (A-B-R1-R2): 3D model (a), experimental [18] (b)



**Figure 7.** Isoleths  $S_1(0.85, 0.15, 0)$ - $S_2(0, 0.15, 0.85)$  (a) and  $CoS-Cu$  (b) of the subsystem  $Co-Cu-CoS-Cu_2S$  ( $A-B-R1-R2$ )  $T-x-y$  diagram 3D computer model

#### 4. Conclusions

The obtained 3D computer model of the  $Co-Cu-CoS-Cu_2S$  subsystem  $T-x-y$  diagram was designed on the basis of the experimental liquidus and solidus surfaces isotherms at temperatures from 1510°C to 800°C. It consists of 82 surfaces and 33 phase regions. The model corresponds to the experimental data and makes it possible to visualize (rotation of 3D figures,  $x-y$  projections, any section) not only liquidus and solidus surfaces, but also other surfaces and phase regions, to understand the crystallization processes, and to calculate the masses balances of the coexisting phases in each of their stages.

#### Acknowledgement

*This work has been performed under the program of fundamental research SB RAS (project 0336-2019-0008) and was partially supported by the Russian Foundation for Basic Research (project 19-38-90035).*

#### References

- [1] F. Kongoli, Y. Dessureault, A.D. Pelton, *Metall. Mater. Trans. B*, 29 (3) (1998) 591-601.
- [2] W. Viljoen, *Phase Relations in the System Cu-Fe-Ni-S and their Application to the Slow Cooling of PGE Matte*, University of Pretoria, Pretoria, 2001, p. 139.
- [3] V. Raghavan, *J. Phase Equilib.*, 25 (5) (2004) 458-461.
- [4] V.I. Kosyakov, E.F. Sinyakova, *Inorg. Mater.*, 48 (7) (2012) 671-675.
- [5] E. Sinyakova, V. Kosyakov, G. Palyanova, N. Karmanov, *Minerals*, 9 (9) (2019) 531.
- [6] V.I. Kosyakov, E.F. Sinyakova, *Inorg. Mater.*, 47 (6) (2011) 660-664.
- [7] R.V. Starykh, S.I. Sineva et al, *Russ. Metall.*, 3 (2009) 263-270; 5 (2009) 447-453; 5 (2010) 448-455; 11 (2010) 1025-1031; 3 (2012) 189-194.
- [8] V.I. Lutsyk, V.P. Vorob'eva, A.E. Zelenaya, *Adv. Mater. Letters*, 10 (1) (2019) 53-57.
- [9] V.I. Lutsyk, V.P. Vorob'eva, *Rus. J. Phys. Chem. A*, 91 (13) (2017) 2593-2599.
- [10] W.J. Schlitt, R.H. Craig, K.J. Richards, *Metall. Mater. Trans. B*, 4 (8) (1973) 1994-1996.
- [11] S.L. Lee, M.J. Larrian, H.H. Kellogg, *Metall. Mater. Trans. B*, 11 (2) (1980) 251-255.
- [12] Y.Y. Chuang, Y.A. Chang, *Metall. Mater. Trans. B*, 13 (3) (1982) 379-385.
- [13] F. Tesfaye, D.K. Lindberg, P. Taskinen, *Proc. EPD Congress 2016 (The Mineral, Metals & Materials Society)*, 14-18 February 2016, Nashville, USA, p. 29-37.
- [14] A. Sugaki, H. Shima, A. Kitakaze, H. Harada, *Econ. Geol.*, 70 (4) (1975) 806-823.
- [15] A. Kitakaze, *Mem. Fac. Eng. Yamaguchi Univ.*, 68 (2) (2017) (55)23-(75)44.
- [16] V.I. Lutsyk, V.P. Vorob'eva, A.M. Zyryanov, S.Ya. Shodorova, *Proc. Takano Intl. Symp. Metals & Alloys Processing (SIPS 2015)*, 4 - 9 October 2015, Antalya, Turkey, 2015, p. 305-326.
- [17] J.R. Craig, D.J. Vaughan, J.B. Higgins, *Econ. Geol.*, 74 (3) (1979) 657-671.
- [18] M.O. Ilatovskaya, R.V. Starykh, S.I. Sinyova, *Metall. Mater. Trans. B*, 45 (5) (2014) 1757-1768.
- [19] M.O. Ilatovskaya, R.V. Starykh, *Metall. Mater. Trans. B.*, 46 (1) (2015) 243-249.
- [20] M.O. Ilatovskaya, S.I. Sinyova, R.V. Starykh, *Calphad*, 59 (2017) 31-39.
- [21] J.E. Morral, S.-L. Chen, *J. Phase Equilib. Diffus*, 38 (3) (2017) 319-331.
- [22] K.A. Khaldoyanidi, *Fazovye diagrammy geterogennykh system s transformatsiyami (Phase Diagrams of Heterogeneous Systems with Transformations)*, Novosibirsk, Institute of Inorganic Chemistry SB RAS, 2004, p. 382 (In Russian).
- [23] A. Prince, *Alloy Phase Equilibria*, Amsterdam-London-N.Y., Elsevier Publ. Comp., 1966, p. 290.
- [24] F.N. Rhines, *Phase Diagrams in Metallurgy. Their development and application*. McGraw-Hill Book Company, MC. New York-Toronto-London, 1956, p. 340.
- [25] R. Vogel, *Die heterogenen Gleichgewichte*. Leipzig: Akademischeverlagellesschaft Geest & Portig, 1959, p. 728.

- [26] D.A. Petrov, *Dvoynye i troinye sistemy (Binary and Ternary Systems)*, Moscow, Metallurgy, 1986, p. 255 (In Russian).
- [27] M. Zakharov, *Diagrammy sostoyaniya dvoynykh i troinykh system (State Diagrams of Binary and Ternary Systems)*, Moscow, Metallurgy, 1990, p. 240 (In Russian).
- [28] V. Lutsyk, A. Zelenaya, V. Vorob'eva, *Abstr. Intern. Conf. on Phase Diagram Calculations and Computational Thermochemistry (Calphad XXXVIII)*, 2009, Prague, Czech Rep., p. 146.
- [29] V.I. Lutsyk, V.P. Vorob'eva, A.E. Zelenaya, *Rus. J. Phys. Chem. A*, 93 (13) (2019) 17-23.
- [30] V.I. Lutsyk, A.M. Zyryanov, A.E. Zelenaya, *Rus. J. Inorg. Chem.*, 53 (5) (2008) 794-799.
- [31] V.I. Lutsyk, V.P. Vorob'eva, *J. Therm. Anal. Calorim.*, 101 (1) (2010) 25-31.
- [32] *Binary Alloy Phase Diagrams*. (Editor T. B. Massalski), American Society for Metals, Ohio, 1986, Vol. 1, Vol. 2.
- [33] *Diagrammy sostoyaniya dvoynykh metallicheskih system (State Diagrams of Binary Metal Systems)* (Editor N.P. Lyakishev) Vol. 2, Mashinostroyeniye, Moscow, 1997, p. 1024 (In Russian).
- [34] M. Muzyk, K.J. Kurzydowski, *J. Min. Metall. Sect. B-Metall.*, 55 (2) B (2019) 271-282.
- [35] V.I. Lutsyk, V.P. Vorob'eva, A.E. Zelenaya, *Solid State Phenomena*, 230 (2015) 51-54.

### 3D KOMPJUTERSKI MODEL T-x-y DIJAGRAMA Co-Cu-CoS-Cu<sub>2</sub>S PODSISTEMA IZNAD 800°C

V. I. Lutsyk <sup>a,b,\*</sup>, V. P. Vorob'eva <sup>a</sup>, A. E. Zelenaya <sup>a</sup>, M. V. Lamueva <sup>a</sup>

<sup>a</sup> Institut za nauku o fizičkim osobinama materijala, Sibirski ogranak Ruske akademije nauka, Ulan-Ude, Rusija

<sup>b</sup> Državni univerzitet Banzarov Burjat, Odsek za hemiju, Ulan-Ude, Rusija

#### Apstrakt

*Predstavljen je trodimenzionalni model T-x-y dijagrama Co-Cu-CoS-Cu<sub>2</sub>S podсистema pri temperaturama iznad 800°C. Pokazano je da se nemešljivost u tečnom stanju u binarnom podsystemu Cu-Cu<sub>2</sub>S unutar trojnog sistema sa Co transformiše u široko dvofazno područje dve nemešljive tečnosti, što prekida krivu Co i Cu<sub>2</sub>S zajedničke kristalizacije. Ispitivane su i posebne odlike strukture solidus površine kobalta prozrokovane nemešljivošću u tečnoj fazi.*

**Ključne reči:** Fazni dijagrami; Nemešljivost; 3D vizualizacija; Metal-sulfid sistemi, Legure kobalta i bakra

